Construction and Building Materials 294 (2021) 123573

Contents lists available at ScienceDirect

Construction and Building Materials

journal homepage: www.elsevier.com/locate/conbuildmat

Advances in the hydration of reactive MgO cement blends incorporating different magnesium carbonates

N.T. Dung [a,b], C. Unluer [c,*]

[a] School of Civil and Environmental Engineering, Nanyang Technological University, 50 Nanyang Avenue, Singapore 639798, Singapore
[b] School of Mechanical Aerospace and Civil Engineering, University of Manchester, M1 3NJ Manchester, United Kingdom
[c] School of Engineering, University of Glasgow, G12 8LT Glasgow, United Kingdom

HIGHLIGHTS

- $Mg(OH)_2$ surface-layers limit the further hydration of reactive MgO cement (RMC).
- Use of magnesium acetate (MA), hydromagnesite (H) and magnesite (M) improved RMC hydration.
- MA and M enhanced the morphology of hydration products.
- Simultaneous use of MA and M improved the compressive strength by 240%.
- Low-crystallinity $Mg(OH)_2$ with a bird nest-like structure was observed in RMC-H samples.

ARTICLE INFO

Article history:
Received 1 January 2021
Received in revised form 19 April 2021
Accepted 4 May 2021

Keywords:
MgO
Hydration
Magnesium carbonates
Performance
Microstructure

ABSTRACT

Hydration of reactive magnesia cement (RMC) is limited by the formation of a $Mg(OH)_2$ surface-layer on unreacted MgO particles. This study improved RMC hydration by using magnesium acetate (MA), along with hydromagnesite (H) and magnesite (M) as RMC replacements. While MA accelerated hydration and resulted in the formation of needle-like artinite, inclusion of M led to rosette-like crystals. The accumulated nucleation and growth of low-crystallinity $Mg(OH)_2$ on H particles in a bird nest-like arrangement was observed for the first time in literature. This low-crystallinity $Mg(OH)_2$ could be prone to carbonation. The replacement of up to 40% RMC with M in the presence of MA improved the compressive strength of RMC samples by 240%. This performance enhancement was supported by microstructure densification via the compact formation of hydrate and carbonate phases, defining M as a feasible partial RMC substitute.

1. Introduction

When compared to Portland cement (PC), reactive MgO cement (RMC) presents lower calcination temperatures and ability to be fully recycled [1–4]. While a ton of RMC results in the emission of 1100 kg of CO_2 (in comparison to 866 kg of CO_2 per ton of PC) [5], its ability to absorb CO_2 permanently could reduce RMC's net emissions and enable it to be considered as a sustainable binder [6–8]. The sequestration of CO_2 within hydrated RMC formulations leads to hydrated magnesium carbonates (HMCs) that provide a dense microstructure and establish a binding network, leading to strength development [9–11]. Some of the common HMCs in RMC formulations are nesquehonite ($MgCO_3{\cdot}3H_2O$), artinite ($Mg_2CO_3(OH)_2{\cdot}3H_2O$) and hydromagnesite ($Mg_5(CO_3)_4{\cdot}(OH)_2{\cdot}4H_2O$) [12,13]. The hydration of RMC, influenced by factors such as the crystal size and surface area of RMC that determine its reactivity, is a critical process in the formation of HMCs. Accordingly, the use of lower temperatures (~750–900 °C) for the calcination of magnesite ($MgCO_3$) leads to the production of RMC with a small crystal size and high surface area, thereby enabling the final product to maintain a high reactivity [2,14].

The reaction between water and anhydrous MgO in RMC forms a $Mg(OH)_2$ surface-layer on the unreacted MgO particles, in addition to the nucleation of $Mg(OH)_2$ (brucite) in the pore space. Because of its linkage with the underlying unhydrated MgO, the structure of $Mg(OH)_2$ forming the surface-layer is different from the precipitated brucite [15]. Accordingly, the $Mg(OH)_2$ surface-layer has a higher solubility than the precipitated brucite. When excess water is available, the $Mg(OH)_2$ surface-layer can dissolve in the free water and precipitate to form brucite away from the underlying MgO, allowing the further hydration of unhydrated

* Corresponding author.
E-mail address: Cise.Unluer@glasgow.ac.uk (C. Unluer).

https://doi.org/10.1016/j.conbuildmat.2021.123573
0950-0618/

MgO. However, the hydration degree of RMC is very low (i.e. ~20–40% at ambient temperatures) [2,16,17] and is limited by the solubility of the $Mg(OH)_2$ surface-layer, which inhibits the continuous hydration of unreacted MgO particles [15,18].

Previous studies reported improvements in the hydration of RMC by using hydration agents and/or high-temperature curing conditions [16,17,19–21]. The most commonly used hydration agents to enhance the hydration of RMC were HCl, $MgCl_2$ and $(CH_3COO)_2Mg$ [19,20]. The use of HCl decreased the alkalinity of the solution, which improved the solubility of MgO and $Mg(OH)_2$ surface-layer, thereby enabling the precipitation of brucite away from the original particles. This improved mechanism provided a higher contact surface area between water and unhydrated MgO grains for the further dissolution of MgO and thus enhanced the hydration degree of RMC. Alternatively, in the presence of $(CH_3COO)_2Mg$ or $MgCl_2$, the CH_3COOMg^+ or Cl^- ions enabled the dissolved Mg^{2+} on the surface layer to migrate away from their original particles and precipitate in the bulk solution to form brucite with a porous structure, as presented in Equations 1–4 [19,22]. This improved mechanism increased the hydration degree of RMC by ~ 54% after 3 days of hydration [17]. On the other hand, the inclusion of $(CH_3COO)_2Mg$, coupled with the use of high-temperature curing at 60 °C, increased the hydration degree of RMC by ~52% just after 1 day [16].

Dissociation of $(CH_3COO)_2Mg$:

$$(CH_3COO)_2Mg_{(aq)} \leftrightarrow 2CH_3COO^-_{(aq)} + Mg^{2+}_{(aq)} \quad (1)$$

Dissolution of MgO:

$$MgO_{(s)} + CH_3COO^-_{(aq)} + H_2O_{(l)} \leftrightarrow CH_3COOMg^+_{(aq)} + 2OH^-_{(aq)} \quad (2)$$

Dissociation of acetate and magnesium ions:

$$CH_3COOMg^+_{(aq)} \rightarrow CH_3COO^-_{(aq)} + Mg^{2+}_{(aq)} \quad (3)$$

Precipitation of $Mg(OH)_2$ due to supersaturation:

$$Mg^{2+}_{(aq)} + 2OH^-_{(aq)} \rightarrow Mg(OH)_{2(s)} \quad (4)$$

In addition to the use of hydration agents, another attempt to facilitate the conversion of MgO to $Mg(OH)_{2(aq,s)}$ involved the inclusion of the nucleation sites within the mixture. Previous studies introduced 0.5–1% (i.e. wt% of binder) hydromagnesite (H) as nucleation seeds within the pore space, which enabled the precipitation of the $Mg(OH)_2$ surface-layer on the seed surfaces as well as the surfaces of MgO particles [23]. This alternative mechanism resulted in a higher content of hydrate phases dispersed throughout the bulk solution instead of precipitating on the original MgO particles. The improvement in the hydration of RMC translated into higher CO_2 absorption within RMC-based formulations [23–25].

Another approach focused on blending RMC with H to improve the hydration degree of RMC and reduce the amount of RMC used [26]. The inclusion of 10–30% H within RMC paste samples significantly accelerated the hydration of RMC at early stages and resulted in a noticeable strength gain (i.e. >24 MPa after 28 days) [15]. This significant increase in strength was attributed to the higher content of hydrate phases with improved morphologies within RMC-H blends. However, the use of commercial H with a high specific surface area led to a high water demand within these RMC-H blends, which significantly lowered their compressive strength (i.e. 28-day compressive strength of ~5 MPa at a water/binder ratio of 1.2) [27].

On the other hand, magnesite (M) has several benefits when compared to many other Mg-carbonate minerals as it does not only have abundant natural resources, but can also be produced via the carbonation of magnesium-based minerals such as serpentine ($Mg_3Si_2O_5(OH)_4$) and forsterite (Mg_2SiO_4) [28–33], making it a much more cost-effective and viable additive than H. Moreover, the production of M via the carbonation of magnesium silicates can significantly reduce the amount of anthropogenic CO_2 [34]. Despite of its many advantages, the combination of M with RMC to improve the hydration degree and reduce the amount of RMC needed for strength development has not been widely reported in the literature.

The introduction of H in RMC mixes was reported to influence the crystallinity and morphology of brucite, resulting in an improvement in the compressive strength of RMC-H blends [15]. However, a further understanding of the change in the properties of brucite and the role of H within these blends is needed. Furthermore, the enhancement of hydration in the presence of a hydration agent and associated improvements in the hydration, and microstructural and mechanical development of RMC-H (i.e. RMC with hydromagnesite) and RMC-M (i.e. RMC with magnesite) blends have not been studied until now. These could be further supported via a detailed study presenting the changes in the pH of the pore solution, phase formations and microstructure of RMC blends, which is yet to be reported.

In line with this gap in the literature, this study aims to improve the hydration of RMC and reduce the CO_2 emissions associated with its incorporation in cementitious blends through the combined use of a hydration agent with different Mg-carbonates. To achieve this, magnesium acetate tetrahydrate (MA, $(CH_3COO)_2Mg{\cdot}4H_2O$) was used as a hydration agent; whereas H and M were introduced as carbonate sources. A comprehensive investigation on the effects of these additives on the hydration, strength gain and associated microstructural properties of RMC blends was performed. The hydration kinetics of RMC in the presence of H/M (i.e. with and without MA) were assessed via pH and isothermal calorimetry measurements. The performance of RMC-H and RMC-M pastes with and without MA was evaluated via the measurement of their compressive strengths at different durations. The reaction products of RMC-H and RMC-M blends with and without MA were investigated by x-ray diffraction (XRD), thermogravimetry (TG) - differential thermogravimetry (DTG) and Fourier Transform infrared (FT-IR) spectroscopy analyses. The influence of each additive on the formation of various hydrate and carbonate phases was analysed using scanning electron microscopy (SEM), backscattered electron (BSE), and energy dispersive x-ray (EDX).

2. Materials and Methodology

2.1. Materials

All the raw materials used in the prepared mix designs were chosen from commercial sources to demonstrate their availability and the feasibility of using the developed formulations in practical applications. Accordingly, commercially available RMC (Richard Baker Harrison - UK), with the chemical composition and physical properties given in Table 1, was used as the main binder. Commercial H and M (Fisher Scientific - UK), used as partial replacements of RMC in the prepared blends, had specific surface areas of 43.5 and 2.3 m^2/g, respectively. The particle size distribution and the morphology of RMC, H and M are shown in Figs. 1 and 2, respectively. MA, with a purity of ≥99% (VWR - Singapore), was employed as a hydration agent to improve the hydration degree of RMC. The XRD patterns of RMC, H and M are presented in Fig. 3.

2.2. Sample preparation and methodology

Paste samples were prepared to study the influence of H and M on the hydration mechanism of RMC with and without MA. The details of the compositions of these paste samples are provided

Table 1
Chemical composition and physical properties of RMC.

	Chemical composition (%)							Physical properties	
	MgO	SiO_2	CaO	R_2O_3	K_2O	Na_2O	LOI	Specific gravity (g/cm^3)	Specific surface area (m^2/g)
RMC	>91.5	2.0	1.6	1.0	–	–	4.0	3.0	16.3

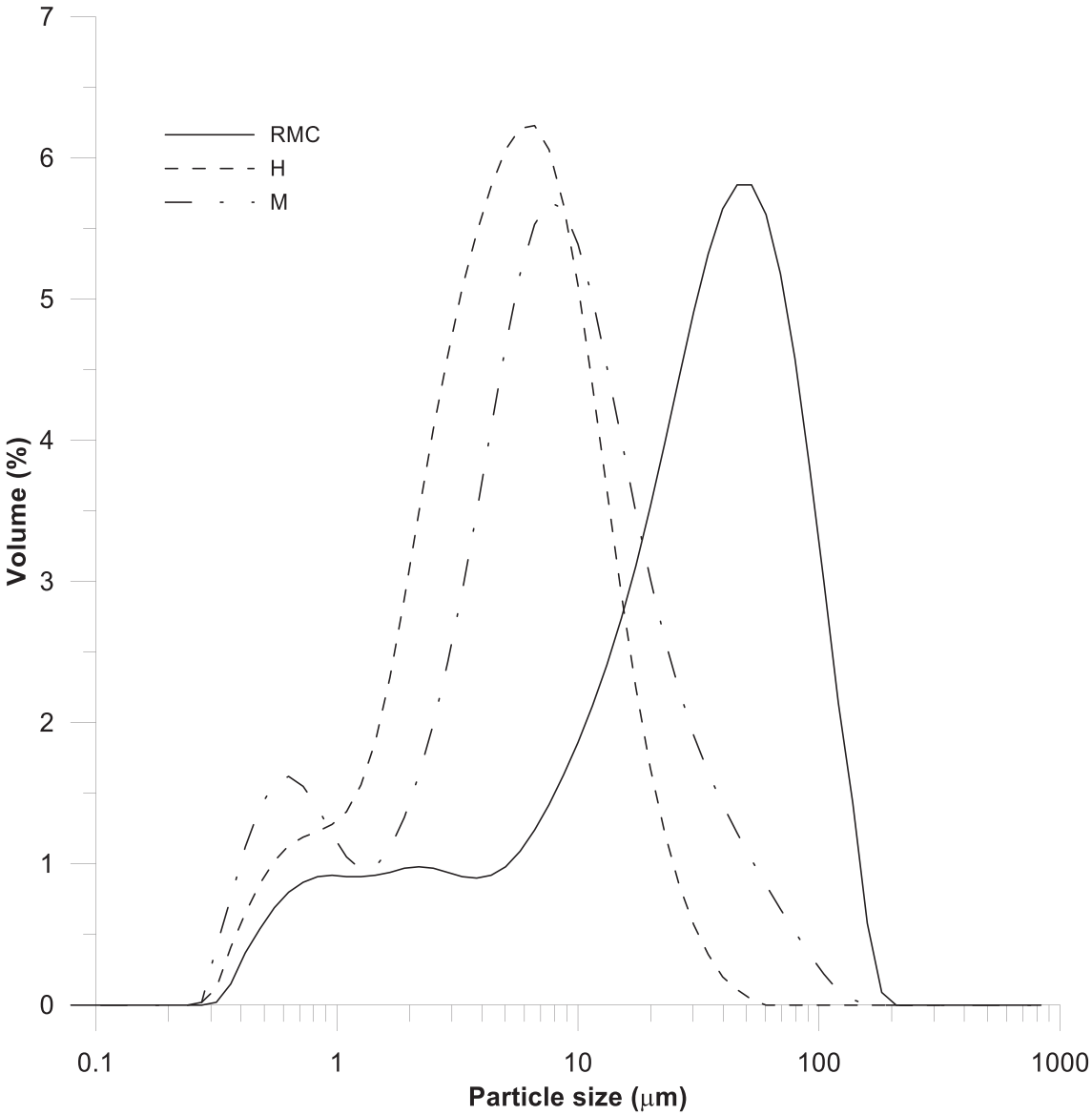

Fig. 1. Particle size distribution of RMC, H and M.

in Table 2. The first set was composed of five samples that did not include any MA. Accordingly, the control sample (CS), whose binder contained 100% RMC, involved a water/binder (w/b) mass ratio of 0.6. Replacement of 20% of RMC with H in sample 20H led to an increase in the w/b ratio to 1.4 due to the high surface area of H, with the goal of achieving a similar workability level as the control sample. These relatively high w/b ratios were in line with those used in the preparation of RMC-H blends in a previous study [27]. The use of any superplasticizers that could potentially reduce the w/b ratio was omitted to avoid any alterations in the hydration of RMC [35], which could interfere with the evaluation of the influence of MA and H on the hydration of RMC-H blends. Alternatively, samples 20 M, 40 M and 60 M, involving the replacement of 20%, 40% and 60% of RMC with M, included lower w/b ratios of 0.6, 0.55 and 0.5, respectively. The differences in the specific surface areas of H and M used in the developed mixes led to variations in the amount of water needed to achieve RMC-H and RMC-M samples with comparable consistencies. The second set involved five samples with the same binder compositions as the first set, the only difference being the use of MA (0.05 M) to accelerate the hydration of RMC.

To prepare the paste samples, the binder was pre-mixed with H/M by using a Kenwood KM 040 mixer prior to introducing the deionized water or MA solution for three minutes. The MA solution was prepared by dissolving MA in deionized water. The prepared pastes were then cast into 5 cm cube moulds, consolidated by a

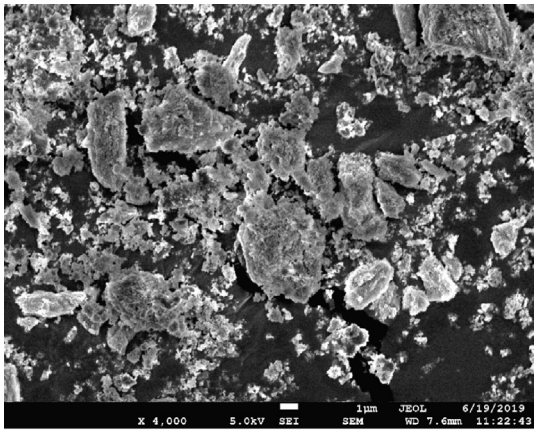

(a)

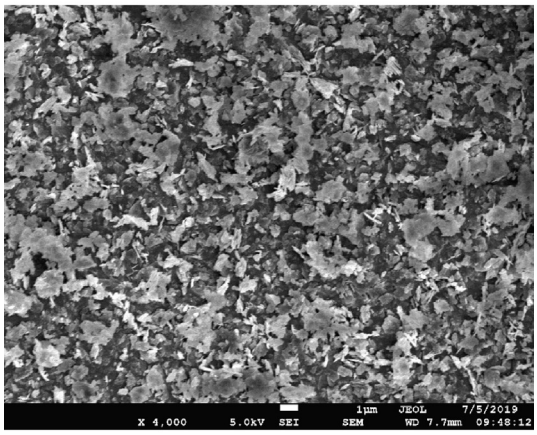

(b)

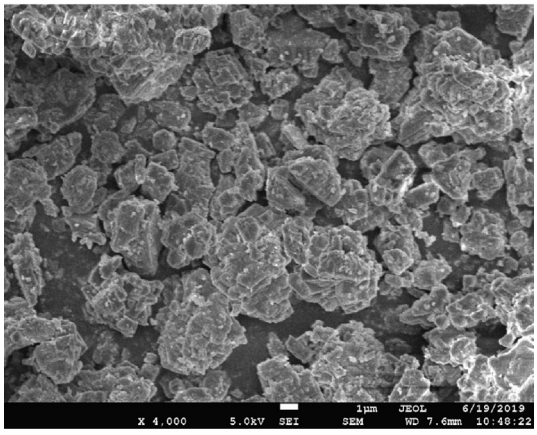

(c)

Fig. 2. SEM images of (a) RMC, (b) H and (c) M.

vibration table for ~10 s and surface finished by a trowel. Afterwards, the 5 cm cube samples were cured under ambient conditions (i.e. ~30 °C and ~80% RH) for 28 days.

2.2.1. pH test

The pH values of the pore solution were determined via the assessment of the diluted pore solution, as suggested by previous studies [36–38]. The hardened pastes were crushed and ground down to pass through a 75 μm sieve. Then, the ground pastes were mixed with distilled water at a water/paste ratio of 5, shaken for 2 min, followed by vacuum filtration. The obtained solution was measured for its pH value by a Mettler Toledo pH meter. The changes in the pH values of each sample were recorded during the first 72 h of hydration.

2.2.2. Isothermal calorimetry

The influence of MA, H and M on the hydration of RMC was demonstrated by the heat flow released by each sample, which was measured at 30 °C according to ASTM C1702 – 15a [39]. To obtain the same conditions as those used during the curing process, the water/MA solution and binders were heated to reach a temperature of 30 °C for 24 h prior to mixing. After mixing, the paste samples were placed in an I-Cal 8000 High Precision Calorimeter to reveal the heat of hydration during the first 24 h.

2.2.3. Compressive strength

The compressive strengths of 5 cm cube samples were tested by a Toni Technik Baustoffprüfsysteme machine with a loading rate of 22 MPa/min on [40]. Three samples were used for each measurement.

2.2.4. Microstructural analysis

Paste specimens intended for microstructural analysis were extracted from cube samples after strength testing, then stored in isopropanol for 24 h, followed by drying under vacuum as suggested by previous studies [41], and ground for XRD and TG-DTG analyses [17].

XRD was operated from 5° to 70° 2θ by a Philips PW 1800 spectrometer using Cu K_α radiation with a scanning rate of 0.04° 2θ/step.

A Perkin Elmer TGA 4000 was linked to a Perkin Elmer FT-IR spectrometer via a TG-IR TL 8000 interface to perform TG-IR measurement as described in [42]. TG was operated from 30 °C to 920 °C at a heating rate of 10 °C/min and under N_2 at a flow rate of 20 ml/min.

A Zeiss Evo 50 microscope was used to obtain SEM images of the reaction products of RMC-H and RMC-M pastes. The elemental distributions were obtained by EDX with an accelerating voltage of 15 kV and a working distance of 15 mm. BSE imaging was also performed to investigate the sample microstructure and the formed phases within the prepared samples. The details of sample preparation for BSE analysis were presented in [43].

3. Results and discussion

3.1. pH

The pH values of the diluted pore solution in hydrated pastes measured over a period of 72 h are shown in Fig. 4. The pH of additional pastes only containing H and M were also presented to investigate the isolated influence of H and M on the hydration of RMC. The pH values of almost all samples reached stable levels after the first 24 h of hydration. The presence of impurities in H and M (e.g. brucite and/or MgO) resulted in an increase in the pH of H (from 10.15 to 10.19) and M (from 9.45 to 9.71) pastes after a few hours of mixing. This was followed by a decline in their pH, which stabilised at ~10.0 and ~9.25 in H and M pastes, respectively.

When the CS was investigated, the initial increase in its pH from 11.54 to 11.64 after 1 h was followed by the gradual precipitation of brucite that reduced the pH to 11.20 after 72 h. The inclusion of H and M, which were expected to accelerate the nucleation and precipitation of brucite, revealed a slight decrease in the pH values in sample 20H (from 10.75 to 10.72) and sample 20 M (from 11.42 to 11.33) after 1 h of mixing. On the other hand, the use of MA led

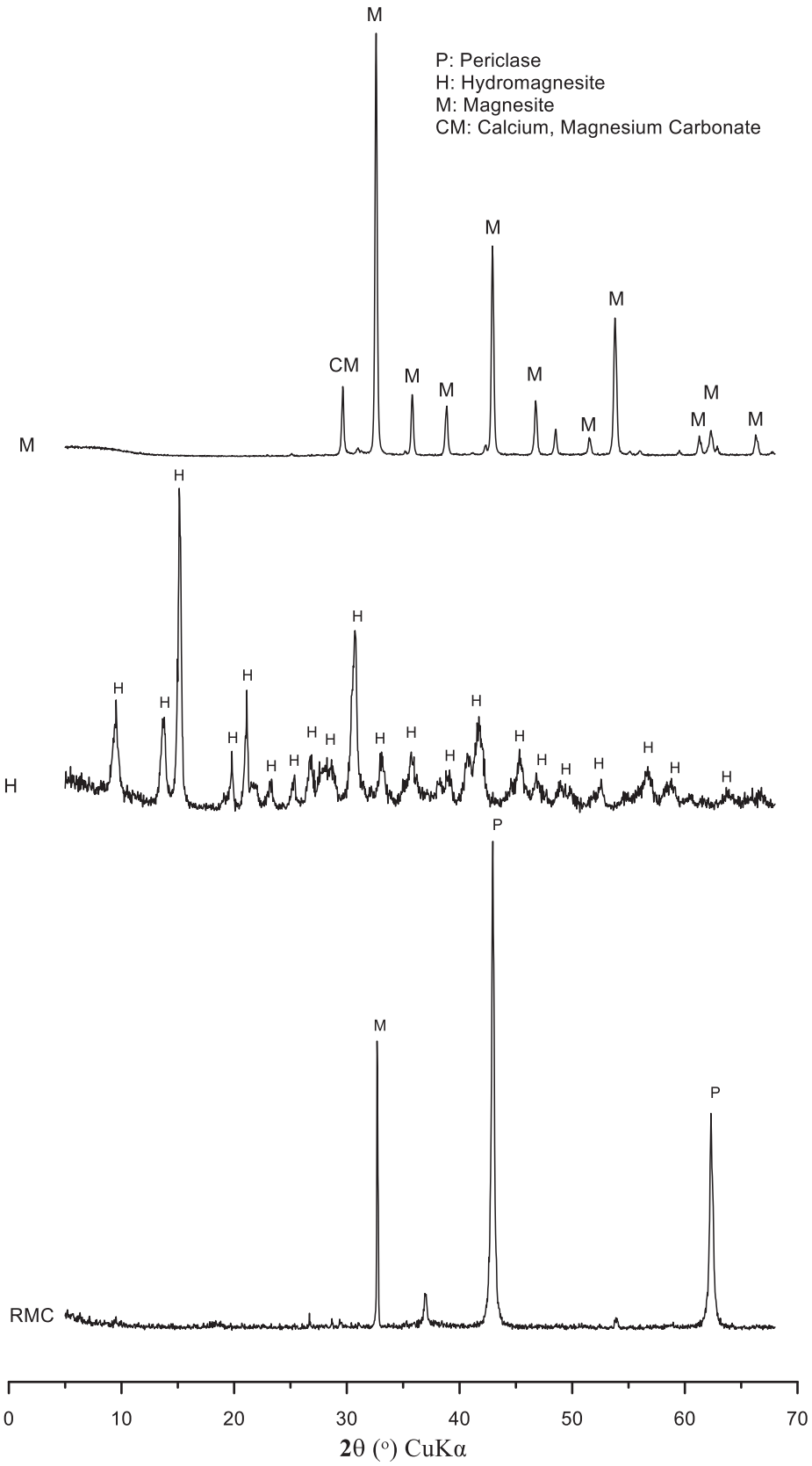

Fig. 3. XRD patterns of RMC, H and M.

to an obvious reduction in the pH values of all samples. For example, a comparison of CS and CS. MA samples highlighted the differences in the pH values of these samples (11.2–11.6 vs. 10.75–11.01), which was attributed to the higher dissolution of MgO in the presence of MA. Accordingly, the combination of MA and H or M resulted in lower pH values in samples 20H.MA

Table 2
Mixture compositions of paste samples.

Mix		Mixture proportion (kg/m^3)				
	Solution/binder	RMC	H	M	Water	MA
CS	0.6	1050	0	0	630	0
20H	1.4	472	118	0	826	0
20 M	0.6	840	0	210	630	0
40 M	0.55	666	0	444	610.5	0
60 M	0.5	472	0	708	590	0
CS.MA	0.6	1050	0	0	623.3	6.7
20H.MA	1.4	472	118	0	817.2	8.8
20 M.MA	0.6	840	0	210	623.3	6.7
40 M.MA	0.55	666	0	444	604	6.5
60 M.MA	0.5	472	0	708	583.7	6.3

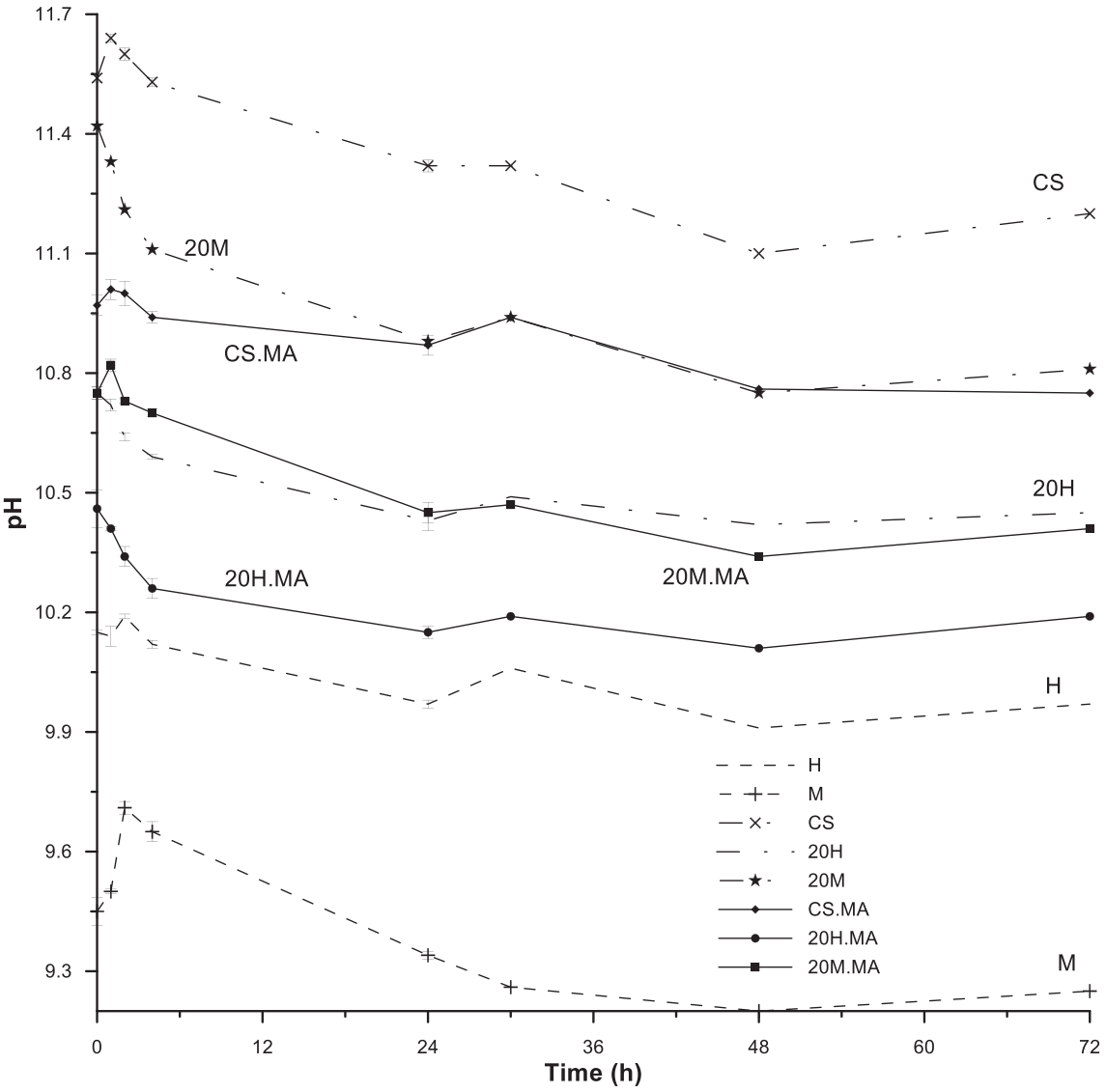

Fig. 4. pH values of the pore solutions of all samples.

(10.11–10.46) and 20 M.MA (10.22–10.82) than the individual use of H or M in samples 20H (10.31–10.75) and 20 M (10.35–11.42). This further decline in the pH of these samples incorporating MA and H or M could be a reflection of the combined effect of both additives on the hydration mechanisms of RMC pastes.

3.2. Isothermal calorimetry

Fig. 5 shows the heat flow released during the first 24 h of hydration in all samples. The exothermic peak, observed after mixing, was an indication of the immediate dissolution of MgO within

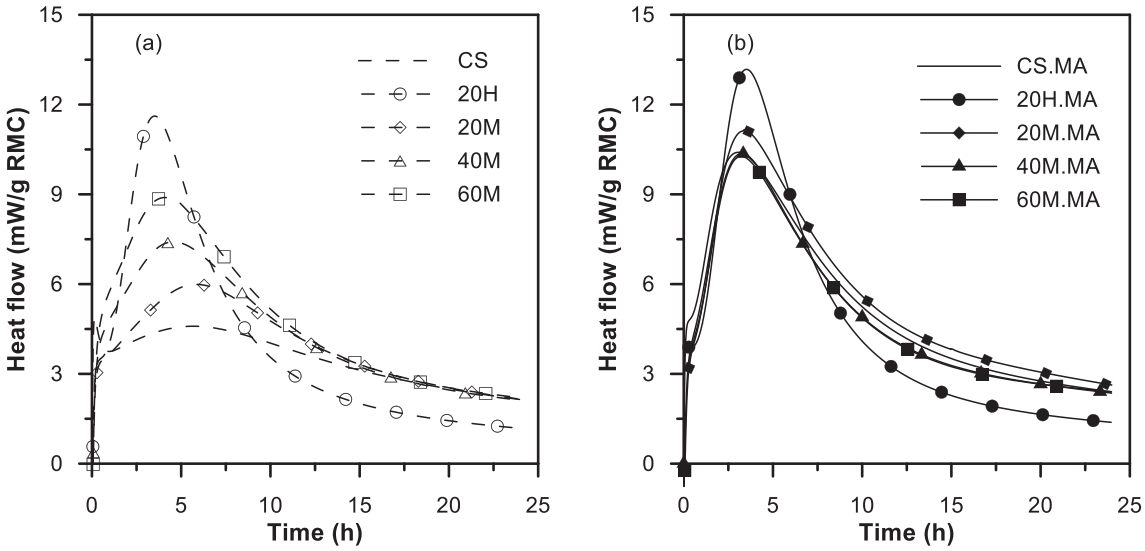

Fig. 5. Heat flow of samples (a) without MA and (b) with MA.

all samples. When compared with the CS, samples including H or M produced higher main peaks, suggesting the acceleration of the hydration of RMC within these samples (Fig. 5(a)). Amongst the first set of samples that did not contain any MA, a direct correlation between the M content and peak intensity and steepness was observed. Accordingly, samples containing higher amounts of M revealed a stronger acceleration in their hydration rates. The higher contents of M could facilitate the dispersion of RMC and provide more nucleation sites for the precipitation of brucite in the pore space, leading to enhanced contact between unhydrated MgO and water, and thereby stimulating the further hydration of RMC [23]. However, regardless of the M content, the most pronounced acceleration in the hydration of RMC was observed in sample 20H. Overall, the inclusion of H or M in RMC blends reduced the dormant period and enabled the appearance of the main peak at an earlier time (i.e. ~3.5 h in sample 20H and ~4.5 h in sample 40 M vs. ~6 h in CS), resulting in an obvious enhancement of the hydration reaction.

The second set of samples containing MA (Fig. 5(b)) revealed hydration peaks with higher intensities than corresponding samples without MA (Fig. 5(a)). This difference confirmed the role of MA in stimulating the dissolution of MgO, which was in agreement with the findings of previous studies [16,17]. However, when compared with sample CS.MA, the use of 20% H or 20% M in samples 20H.MA and 20 M.MA had a relatively small accelerating effect on the hydration of RMC. Differing from the first set, increasing the M content from 20% to 40–60% did not have any notable effect on the hydration of RMC in samples 40 M.MA and 60 M.MA. These results highlighted the prevailing role of MA in enhancing the hydration of RMC binders, irrespective of the presence of other carbonate additives.

3.3. Compressive strength

Fig. 6 presents the compressive strengths of samples over 28 days of hydration. The CS (Fig. 6(a)) produced very low compressive strengths (5 MPa after 28 days of hydration). When compared with the CS, the use of M in samples 20 M (12 MPa) and 40 M (8 MPa) led to higher 28-day compressive strengths. However, increasing the M content to 60% in sample 60 M resulted in similar

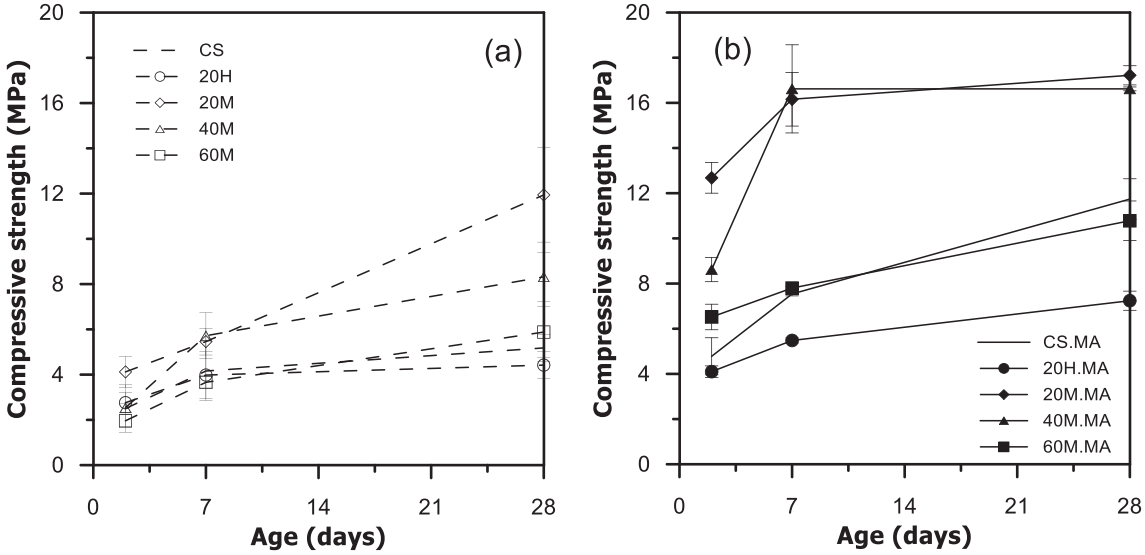

Fig. 6. Compressive strength of samples (a) without MA and (b) with MA.

strengths to those of the CS. Despite its obvious effect in accelerating the hydration of RMC (Fig. 5(a)), the use of H in sample 20H revealed comparable strengths with those of the CS. This inconsistency in the strength results could be associated with the higher w/b ratio of this sample, which may have increased its porosity, thereby leading to lower strengths.

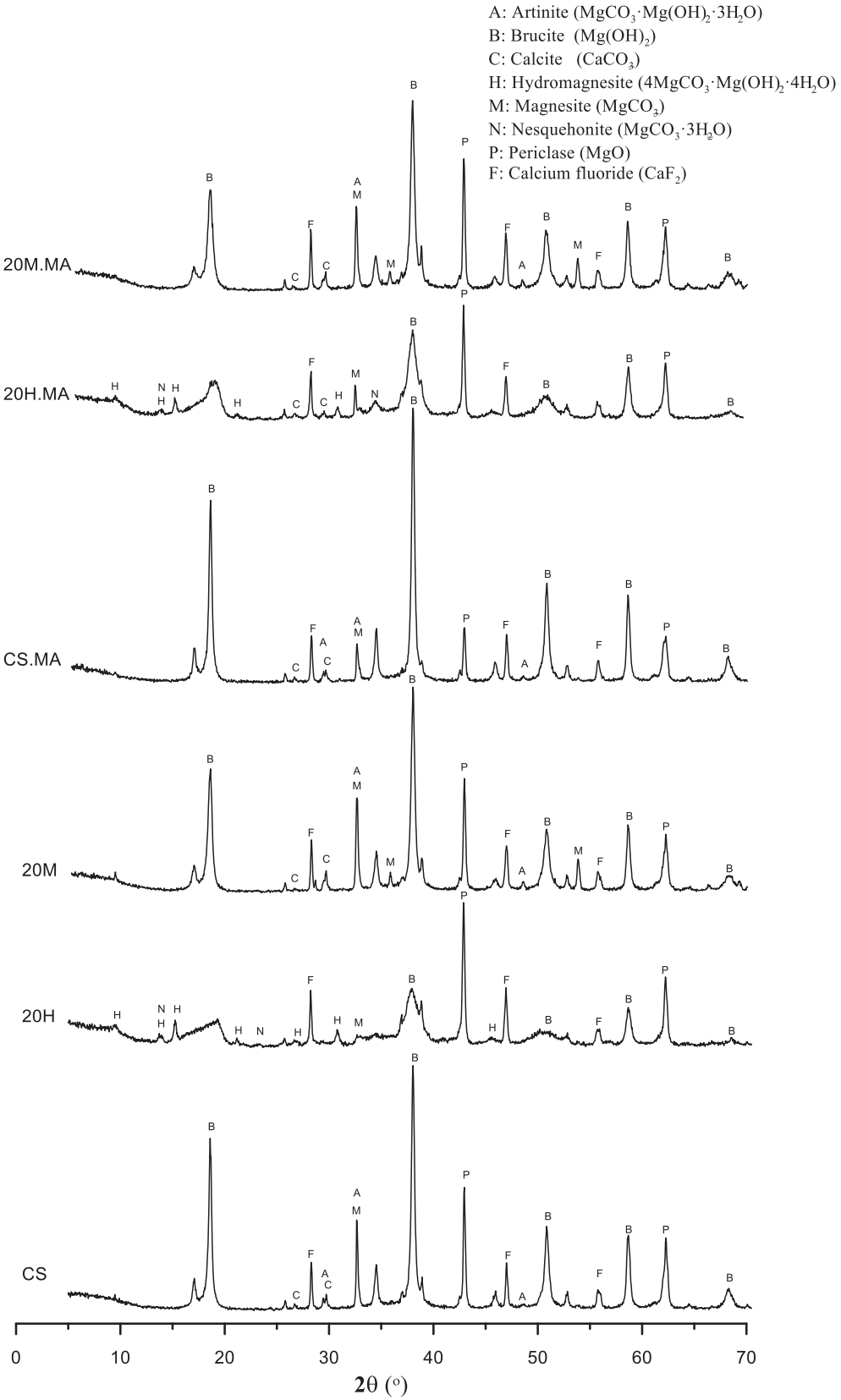

Fig. 7. XRD patterns of samples at 7 days.

In line with the trends observed in isothermal calorimetry, the use of MA enhanced the hydration process and significantly improved the compressive strengths of all samples, resulting in higher strengths than corresponding samples without any MA (Fig. 6(b)). While MA had an obvious influence in increasing the strength, a similar trend as the one observed in the first set (i.e. without any MA) was revealed by the second set (i.e. with MA) of samples in terms of the roles of M and H. Accordingly, among samples containing MA, sample 20H.MA produced the lowest compressive strength (7 MPa after 28 days). Since it had revealed the highest hydration peak in Fig. 5(b), the low performance of this sample could be linked with its high water content. The influence

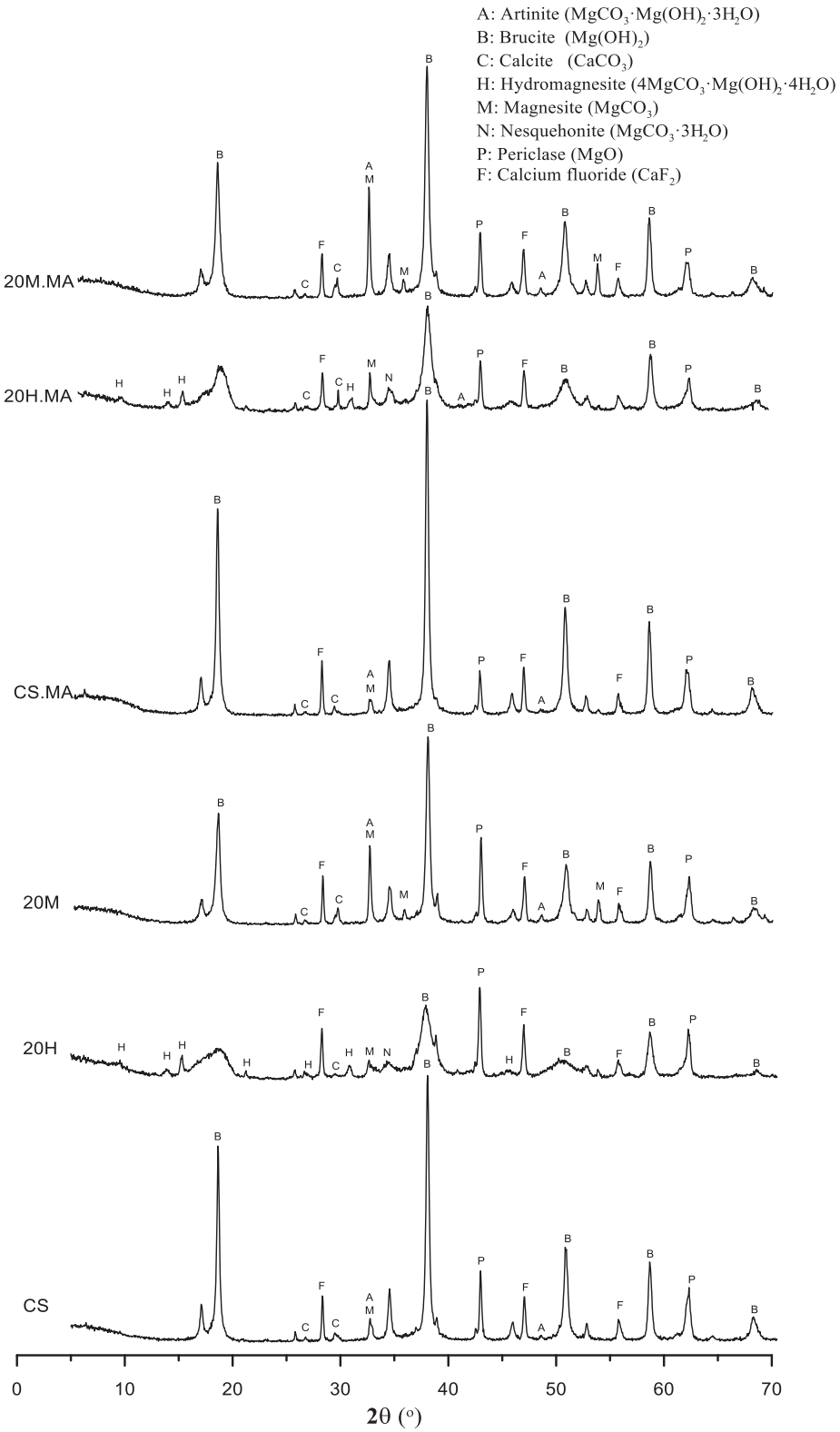

Fig. 8. XRD patterns of samples at 28 days.

of MA on enhancing the mechanical performance of RMC-H samples was highlighted by the higher strengths of sample 20H.MA than those reported in the literature for comparable RMC-H blends (7 vs. 5 MPa at 28 days), despite its higher w/b ratio (1.4 vs. 1.2) [27]. Alternatively, samples 20 M.MA and 40 M.MA achieved the highest strengths amongst all samples, both reaching 17 MPa at 28 days. Amongst these two samples, 20 M.MA revealed a higher early (2-day) strength than 40 M.MA (13 vs. 9 MPa), which could be due to the higher brucite content within the former. The lower w/b ratio of sample 40 M.MA led to equivalent strengths with sample 20 M.MA, despite the lower RMC content of the former. Increasing the M content to 60% in sample 60 M.HA did not result

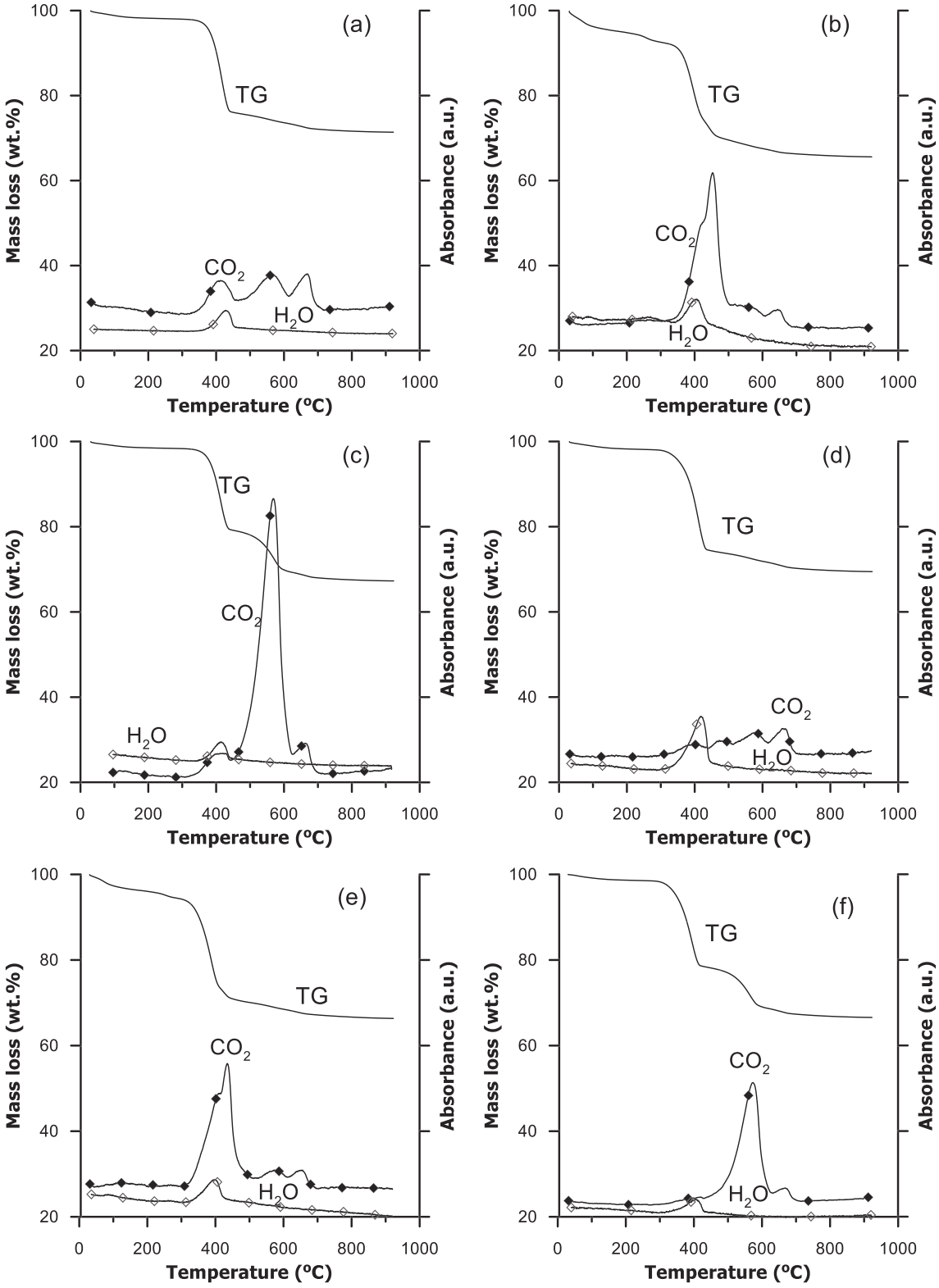

Fig. 9. TG-IR results after 7 days of hydration of samples (a) CS, (b) 20H, (c) 20 M, (d) CS.MA, (e) 20H.MA and (f) 20 M.MA.

in any improvements and revealed a similar compressive strength as sample CS.MA (~11 MPa at 28 days), despite its lowest w/b ratio. These observations could be attributed to the lower initial RMC content within sample 60 M.HA in comparison to samples 20 M.MA and 40 M.MA.

Overall, the strength results highlighted the effectiveness of MA in enhancing the performance of the prepared formulations, which resulted in 140% increase in the 28-day strength. When coupled with the use of 20–40% M in samples 20 M.MA and 40 M.MA, the strength further went up, producing 240% higher 28-day strength results than the CS.

3.4. Xrd

The XRD data of selected samples after 7 and 28 days of hydration are shown in Figs. 7 and 8, respectively. Unhydrated periclase (MgO, 42.9° 2θ) was observed in all samples. A comparison of the residual periclase peaks amongst different samples, with reference to the internal standard, CaF_2 (28.2° 2θ) [44], indicated the lower intensity of unhydrated periclase in the presence of MA. This reduction in periclase content indicated the role of MA in accelerating the hydration of RMC. A further decrease in the intensity of unhydrated periclase over time indicated the progress of hydration as curing proceeded from 7 to 28 days. The main reaction products of the CS included brucite ($Mg(OH)_2$, 18.6°, 38.1° and 50.9° 2θ), artinite ($Mg_2CO_3(OH)_2{\cdot}3H_2O$, 32.8° 2θ) and calcite ($CaCO_3$, 29.7° 2θ). The formation of brucite, artinite and calcite within the CS was associated with the hydration of MgO (and other impurities such as CaO) within RMC and subsequent carbonation reaction involving atmospheric CO_2, as demonstrated in Eqs. (5)–(8).

The hydration of MgO to form brucite:

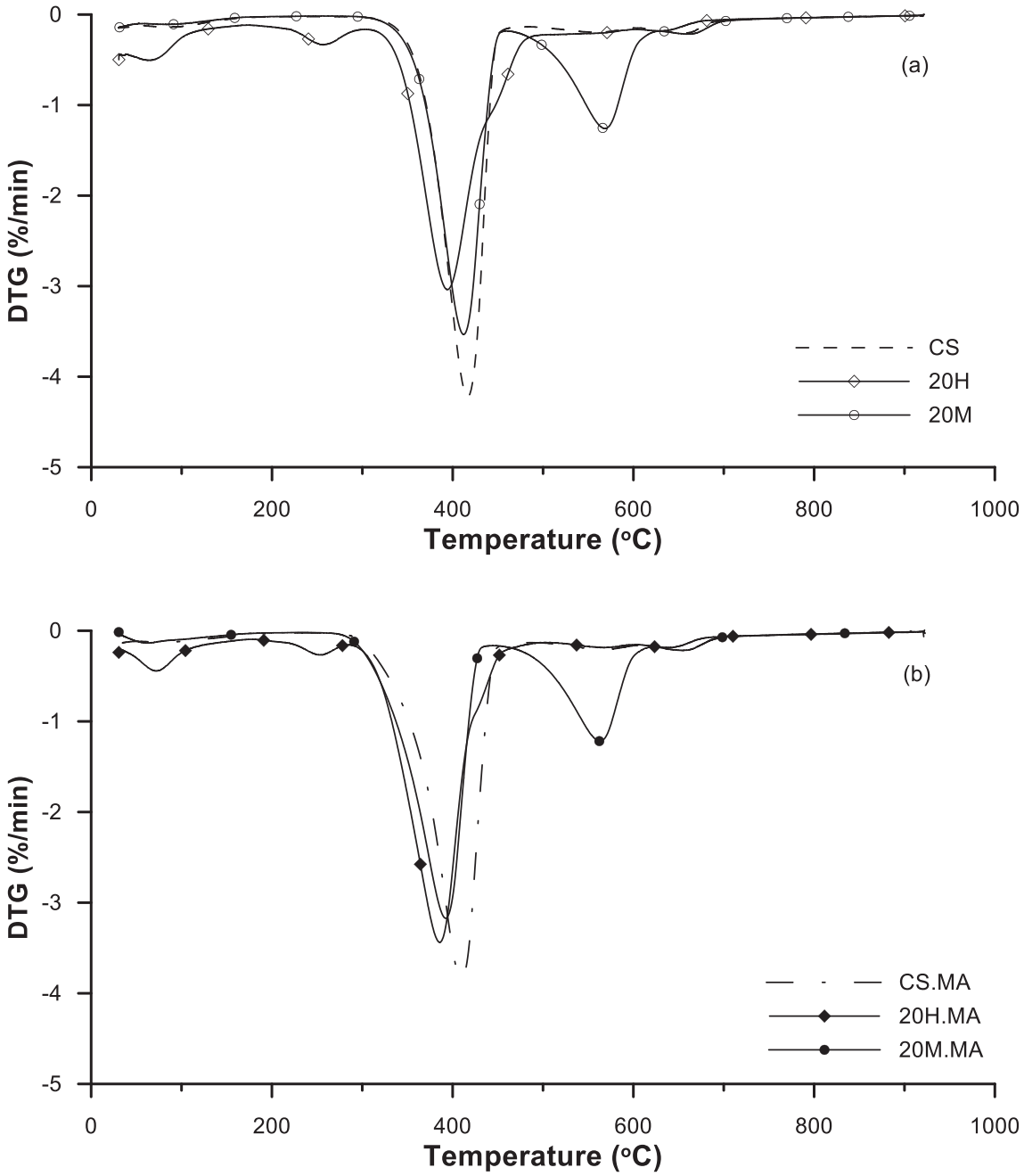

Fig. 10. DTG results after 7 days of hydration of samples (a) without MA and (b) with MA.

$$MgO + 2H_2O \rightarrow Mg(OH)_2 \quad (5)$$

The carbonation of brucite to form artinite:

$$2Mg(OH)_2 + CO_2 + 2H_2O \rightarrow MgCO_3 \cdot Mg(OH)_2 \cdot 3H_2O \quad (6)$$

The carbonation of CaO (present as an impurity in RMC) to form calcite:

$$CaO + H_2O \rightarrow Ca(OH)_2 \quad (7)$$

$$Ca(OH)_2 + CO_2 \rightarrow CaCO_3 + H_2O \quad (8)$$

Despite enhancing the hydration reaction, the inclusion of MA or M in RMC formulations did not change the composition of the hydration products. Alternatively, the use of H influenced the

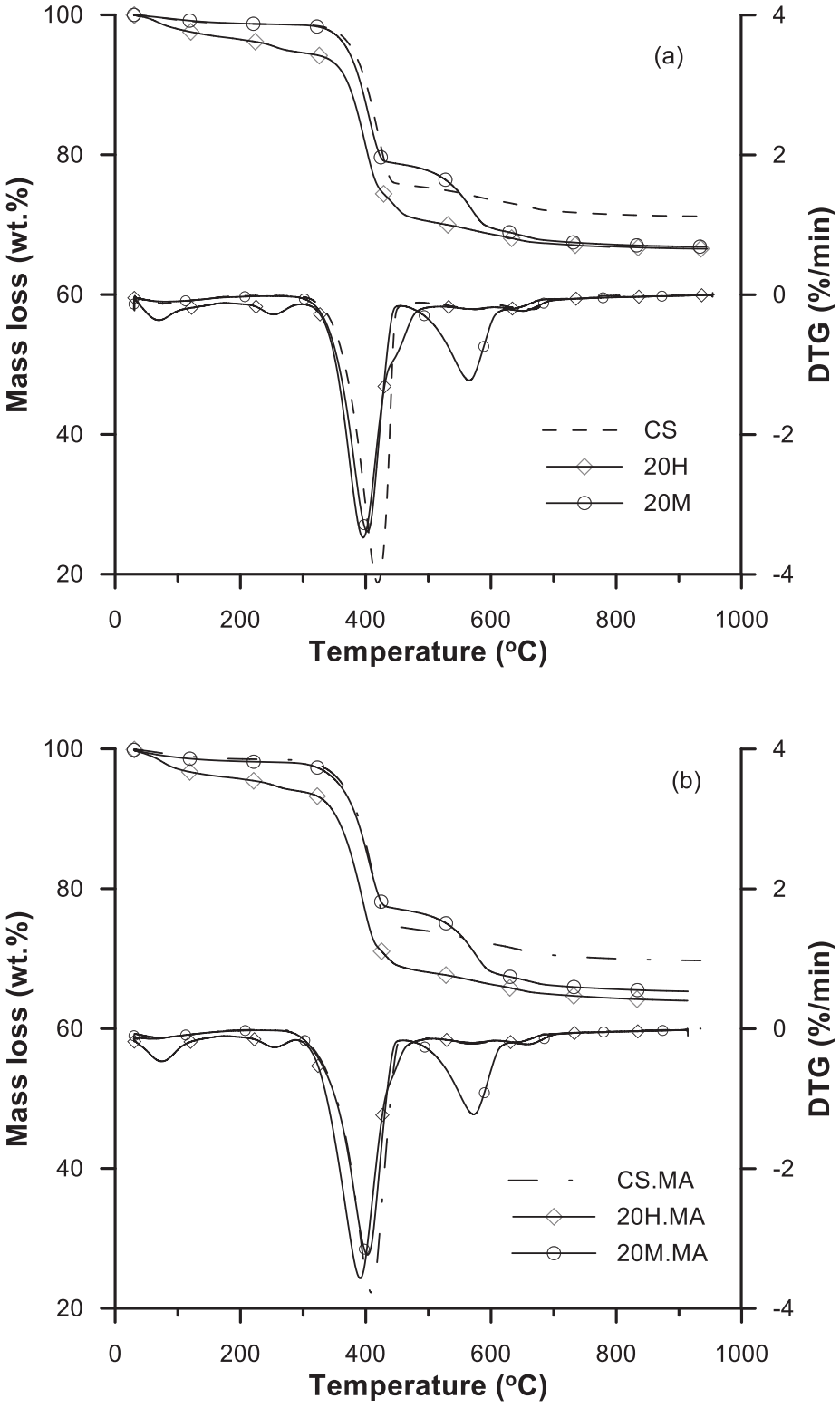

Fig. 11. TG and DTG results after 28 days of hydration of samples (a) without MA and (b) with MA.

hydrate and carbonate phases within samples 20H and 20H.MA. In addition to the phases observed in the CS, hydromagnesite ($4MgCO_3{\cdot}Mg(OH)_2{\cdot}4H_2O$, 15.2° 2θ) and nesquehonite ($MgCO_3{\cdot}3H_2O$, 13.7° and 34.4° 2θ) were observed in samples 20H and 20H.MA. XRD patterns of RMC-based samples usually reveal HMC peaks with low intensities, especially under ambient conditions [45]. Furthermore, the artinite peak at 32.8° 2θ was more obvious in sample 20H.MA than it was in sample 20H. A shift in the brucite peak, originally at 18.6° 2θ, to 19.4° 2θ, was observed in sample 20H; whereas the broadening of the same peak at ~ 19° 2θ was seen in sample 20H.MA after 7 days of hydration.

Another obvious change within the phase formations facilitated by the inclusion of H was the transformation of brucite peaks from their originally crystalline structure into a broader peak at 38.1° 2θ and a hump at 50.9° 2θ. In line with previous research [15], these poorly crystalline phases of brucite revealed by sample 20H at 7 days became sharper at 28 days. Differing from the low crystallinity brucite, the use of MA enhanced the hydration process, resulting in brucite with a higher crystallinity in sample 20H.MA when compared to 20H. As the decomposition of H and its reaction with hydrated MgO is not likely to result in nesquehonite, the formation of these carbonates could be attributed to the carbonation of hydrated MgO under ambient conditions. Within these systems, the low crystallinity $Mg(OH)_2$ observed in samples incorporating H could be more prone to carbonation than brucite crystals. These findings differed from those presented in previous studies [15,27], where the formation of nesquehonite was not observed in RMC-H blends. While this could be due to lack of carbonation under the sealed conditions used in these studies, the formation of nesquehonite under ambient conditions was reported earlier [17], where the hydration of RMC samples was accelerated by using hydration agents (i.e. HCl and $MgCl_2$).

3.5. TG-IR & Dtg

The TG-IR curves of selected samples after 7 days of hydration are shown in Fig. 9. The main mass loss observed in the CS took place at ~ 420 °C, corresponding to the dehydroxylation of brucite and decomposition (i.e. dehydroxylation and decarbonation) of some HMCs. This was followed by the decarbonation of the remaining carbonate phases at ~ 580 °C and ~ 680 °C. The inclusion of H in sample 20H revealed an additional mass loss due to dehydration at < 300 °C and a shift in the main mass loss from ~ 420 °C to ~ 480 °C. Alternatively, while the inclusion of M in sample 20 M did not result in the dehydration observed in sample 20H at < 300 °C, a strong mass loss due to decarbonation was observed at ~ 580 °C. This mass loss was mainly associated with the decomposition of $MgCO_3$.

The incorporation of MA in sample CS.MA resulted in a higher mass loss at ~ 410 °C than CS due to dehydroxylation. This increased mass loss was an indication of the enhanced hydration of RMC and the associated conversion of MgO into brucite, without changing the general decomposition pattern. However, the simultaneous inclusion of MA with H or M resulted in similar decomposition patterns within samples 20H.MA and 20H; and samples 20 M.MA and 20 M.

The DTG results of the same samples after 7 days of hydration are shown in Fig. 10, whereas their combined TG-DTG curves after 28 days of hydration are shown in Fig. 11. According to the IR results, the endothermic peaks at < 300 °C, 300–400 °C and > 400 °C corresponded to the dehydration, dehydroxylation and decarbonation processes, respectively. In line with previous research [27], two obvious mass loss steps corresponding to dehydration, whose peaks were located at ~ 90 °C and ~ 250 °C, were observed in sample 20H (Fig. 10(a) and Fig. 11(a)). Since the dehydration of pure H occurred at ~ 250 °C [46,47] and the hydration of pure RMC (i.e. CS) did not result in any obvious dehydration peaks, the dehydration peak at ~ 90 °C observed in sample 20H could correspond to the bonding water, which was associated with the improved microstructure and compressive strength in RMC-H samples reported in a previous study [15]. Another study [27] hypothesised that this additional bonding water represented the poorly crystalline phases in RMC-H blends. The absence of poorly crystalline phases and the dehydration peak at ~ 90 °C in sample 20 M strengthened this hypothesis. The appearance of these two mass loss steps in sample 20H.MA (Fig. 10(b) and Fig. 11(b)) suggested that the use of MA did not alter the bonding water of hydrate phases in the RMC-H blends.

The decomposition of all hydrate/carbonate phases led to a certain mass loss, which was calculated by the areas obtained by the deconvolution of DTG results, as shown in Table 3. The dehydroxylation of brucite and HMCs was responsible for the highest proportion of mass loss. While the value for dehydroxylation within the CS was 22.1% after 7 days of hydration, this value was lower for 20H (19.3%) and 20 M (19.8%) samples. Considering these samples involved lower RMC contents than the CS (80% vs. 100% RMC) as 20% of RMC was replaced by H or M, even lower mass losses (17.8% for 20H and 17.1% for 20 M) would be expected if the hydration process was not enhanced in the presence of these additives.

The use of MA increased the mass loss due to dehydration and dehydroxylation within samples CS.MA, 20H.MA and 20 M.MA when compared with the corresponding samples CS, 20H and 20 M, respectively. These enhancements in mass loss were consistent with findings of isothermal calorimetry, which revealed a rise in the heat evolved in the presence of these

Table 3
Mass loss of paste samples after 7 and 28 days of curing, measured by TG-DTG.

Duration	Mix	Mass loss (wt.%)			
		Dehydration	Dehydroxylation	Decarbonation	Total
7 days	CS	1.1	22.1	6.3	29.5
	20H	5.2	19.3	9.4	34.0
	20 M	1.0	19.8	12.0	32.8
	CS.MA	1.4	22.5	7.6	31.5
	20H.MA	5.3	19.5	9.4	34.1
	20 M.MA	1.4	20.9	11.8	34.0
28 days	CS	1.0	21.9	6.8	29.6
	20H	5.5	19.0	10.0	34.5
	20 M	1.3	20.0	12.3	33.6
	CS.MA	1.6	21.5	7.9	31.1
	20H.MA	5.7	20.5	10.3	36.5
	20 M.MA	1.6	21.1	12.1	34.8

additives. The slight but consistent increase in the mass loss results from 7 to 28 days indicated the continuous progress in hydration/carbonation with time, albeit at a slower rate after the first 7 days. Amongst these, mass loss due to dehydroxylation remained relatively constant. Alternatively, the rise in carbonation over time was revealed by the increase in the mass loss due to decarbonation in all samples, indicating the gradual carbonation of Mg-phases. The combination of the improvements in the hydration reaction, along with the progressive formation of carbonate phases, were responsible for the increase in the compressive strength results over time.

3.6. Microstructure

Fig. 12 shows the microstructures of selected samples after 7 days of hydration. The CS (Fig. 12(a)) revealed a sparsely hydrated microstructure, in which the scarce presence of very small (~0.3 μm) disk-like crystals was observed. When compared with the CS, the combination of RMC and H in sample 20H (Fig. 12(b)) resulted in crystal formations with improved morphologies, as revealed by the agglomeration of disk-like crystals (diameter of ~ 1–1.5 μm). Alternatively, the use of M in sample 20 M (Fig. 12(c)) resulted in the dense formation of carbonate

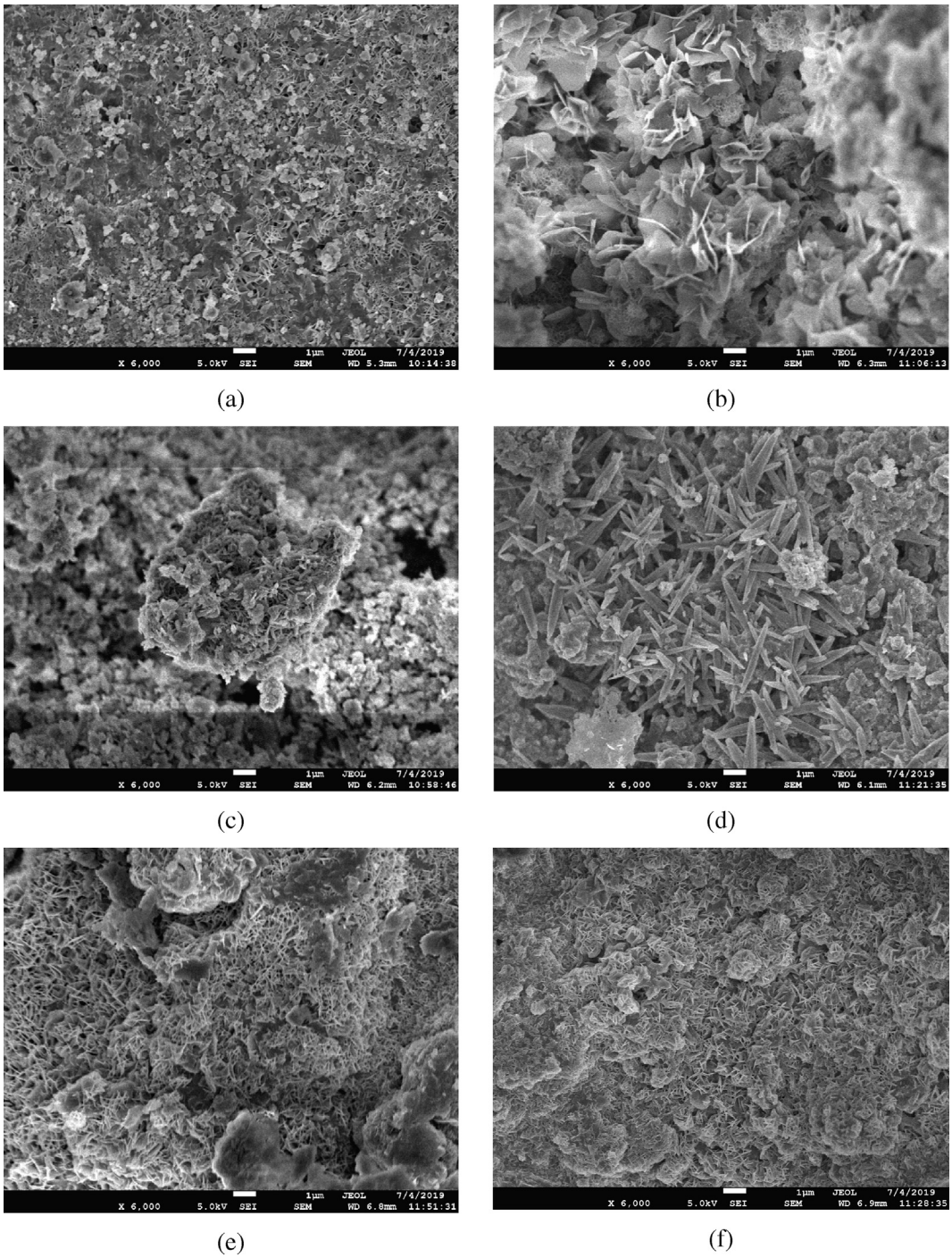

Fig. 12. SEM images after 7 days of hydration of samples (a) CS, (b) 20H, (c) 20 M, (d) CS.MA, (e) 20H.MA and (f) 20 M.MA.

agglomerates with various morphologies, including artinite with a length of ~ 1 μm.

The sole incorporation of MA in sample CS.MA (Fig. 12(d)) led to a very notable change in the sample microstructure, in which the formation of needle-like artinite crystals with a length of ~ 2–3 μm was observed. This was followed by the simultaneous inclusion of MA and H or M in samples 20H.MA (Fig. 12(e)) and 20 M. MA (Fig. 12(f)), where the improvement of hydration via the use of these additives revealed the formation of dense microstructures composed of various reaction products. When compared to the other samples analysed after 7 days of hydration, sample 20 M. MA produced the densest microstructure occupied by rosette-like hydrate and carbonate phases, which could explain its higher strengths than others.

Fig. 13 shows the microstructures of selected samples after 28 days of hydration. An obvious shift in the microstructure of samples was observed with an increase in curing time (7 vs. 28 days). Accordingly, the microstructure of the CS (Fig. 13(a)) shifted from its previously uneventful composition (i.e. at 7 days) to one in which the growth of large rosette-like crystals (i.e. bru-

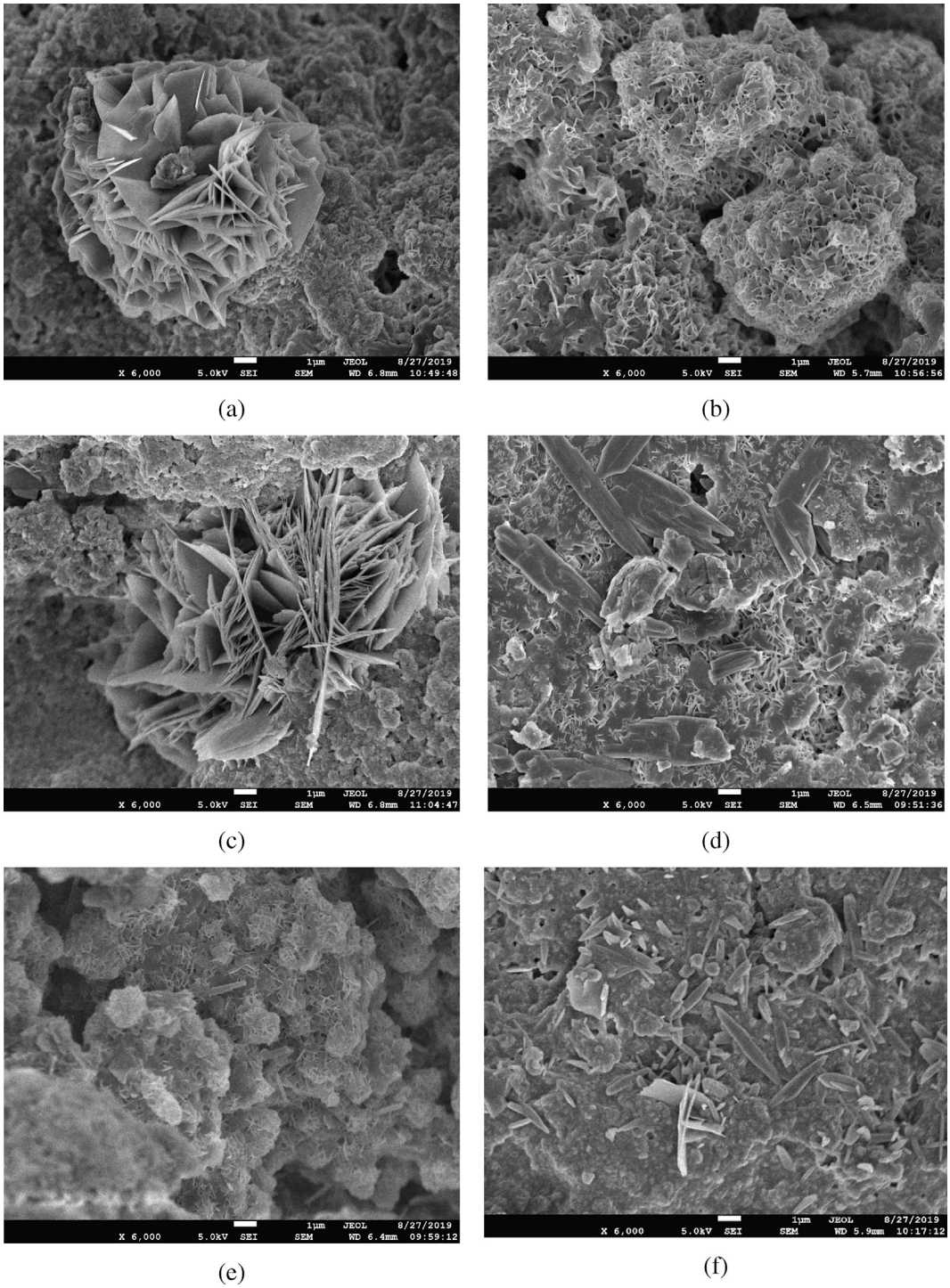

Fig. 13. SEM images after 28 days of hydration of samples (a) CS, (b) 20H, (c) 20 M, (d) CS.MA, (e) 20H.MA and (f) 20 M.MA.

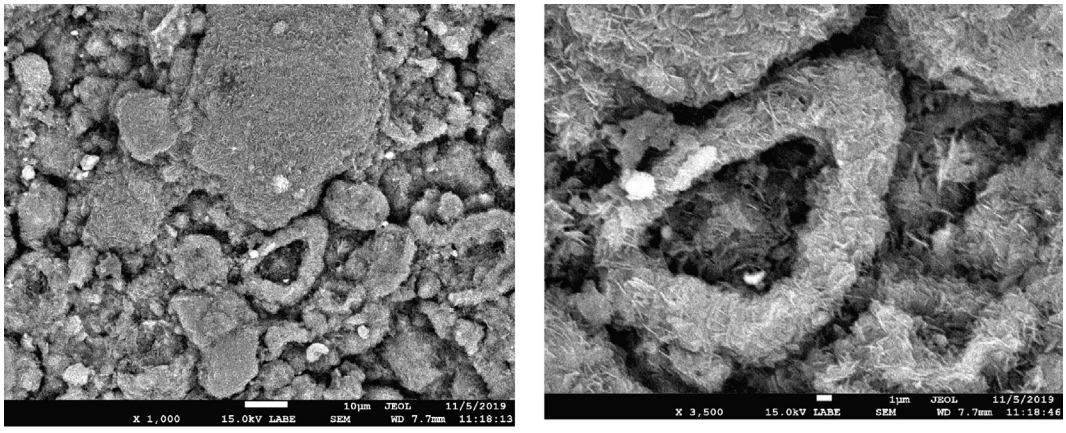

Fig. 14. Microstructure of sample 20H at 28 days.

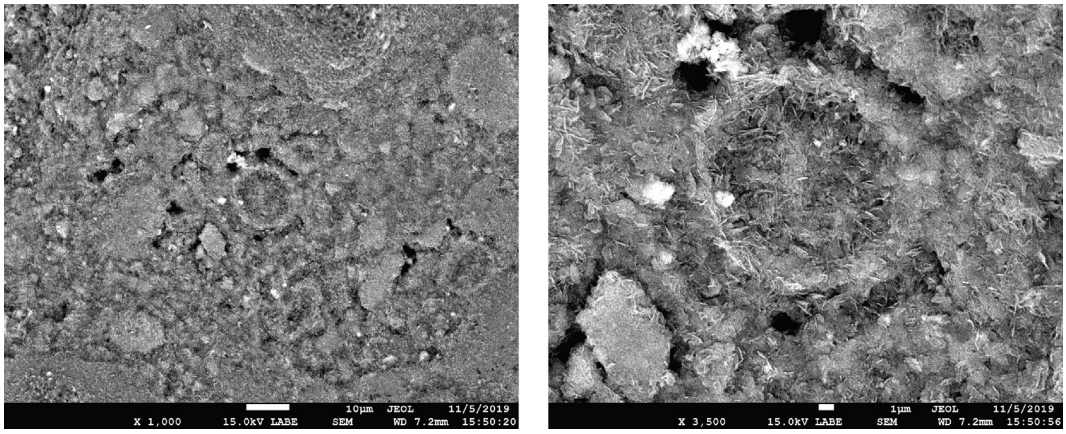

Fig. 15. Microstructure of sample 20H.MA at 28 days.

cite) with a diameter of ~ 2–3 μm was spotted. These formations were associated with the continuous hydration of RMC. The use of H in sample 20H (Fig. 13(b)) revealed the growth of agglomerated disk-like crystals within a porous microstructure. When compared with the CS, the inclusion of M in sample 20 M (Fig. 13(c)) improved the morphology of the reaction products via the formation of large rosette-like crystals containing sharp edges, with a diameter of up to ~ 5 μm.

The use of MA in sample CS.MA (Fig. 13(d)) resulted in a notable transition in sample microstructure from a composition of rosette- or disk-like crystal agglomerates to microstructures involving the combination of various phases, including the appearance of needle-like crystals with a length of ~ 6 μm. These needle structures were surrounded by agglomerated disk-like crystals. Alternatively, the incorporation of H in sample 20H.MA (Fig. 13(e)) resulted in the formation of needle-like crystals indicating the presence of nesquehonite with a length of ~ 1.5 μm, albeit in a porous microstructure, which could be linked with the high amount of water used in this mix. Differing from the other samples, the simultaneous inclusion of MA and M in sample 20 M.MA (Fig. 13 (f)) produced a denser microstructure composed of disk-like crystals with a diameter of ~ 2–3 μm and needle-like artinite with a length of up to ~ 3 μm, which was in line with the outstanding mechanical performance of this sample (Fig. 6).

A further investigation of the microstructures of samples 20H (Fig. 14) and 20H.MA (Fig. 15) at 28 days revealed the formation of a bird nest-like arrangement, where the disk-like crystals surrounded the round H seeds. This unique formation, reported for the first time in literature within the context of RMC formulations, was composed of hydrated MgO and carbonates, as seen in the elemental analysis results (Fig. 16). It was speculated that the additional bonding water, with a thermal dehydration at ~ 90 °C, could have enabled the bond between brucite and H to form this novel structure. Accordingly, unlike the highly crystalline phases observed in other samples, the use of H within RMC formulations provided additional nucleation sites, around which brucite and H bonded together to form a bird nest-like structure under ambient conditions, thereby changing the crystallinity of brucite. Another potential cause for the formation of this structure could be associated with the removal of excess water used in RMC-H blends, which would lead to a porous structure. Thermodynamic calculations on similar blends suggested the formation of an intermediate phase between hydromagnesite ($(Mg_5(CO_3)_4{\cdot}(OH)_2{\cdot}4H_2O)$) and brucite ($Mg(OH)_2$) [15]. Fig. 16 indicates the different distribution of C within this structure, showing the variations in the chemical composition of the bird nest-like structure. These alterations could explain the changes in the peak structures revealed by the XRD patterns.

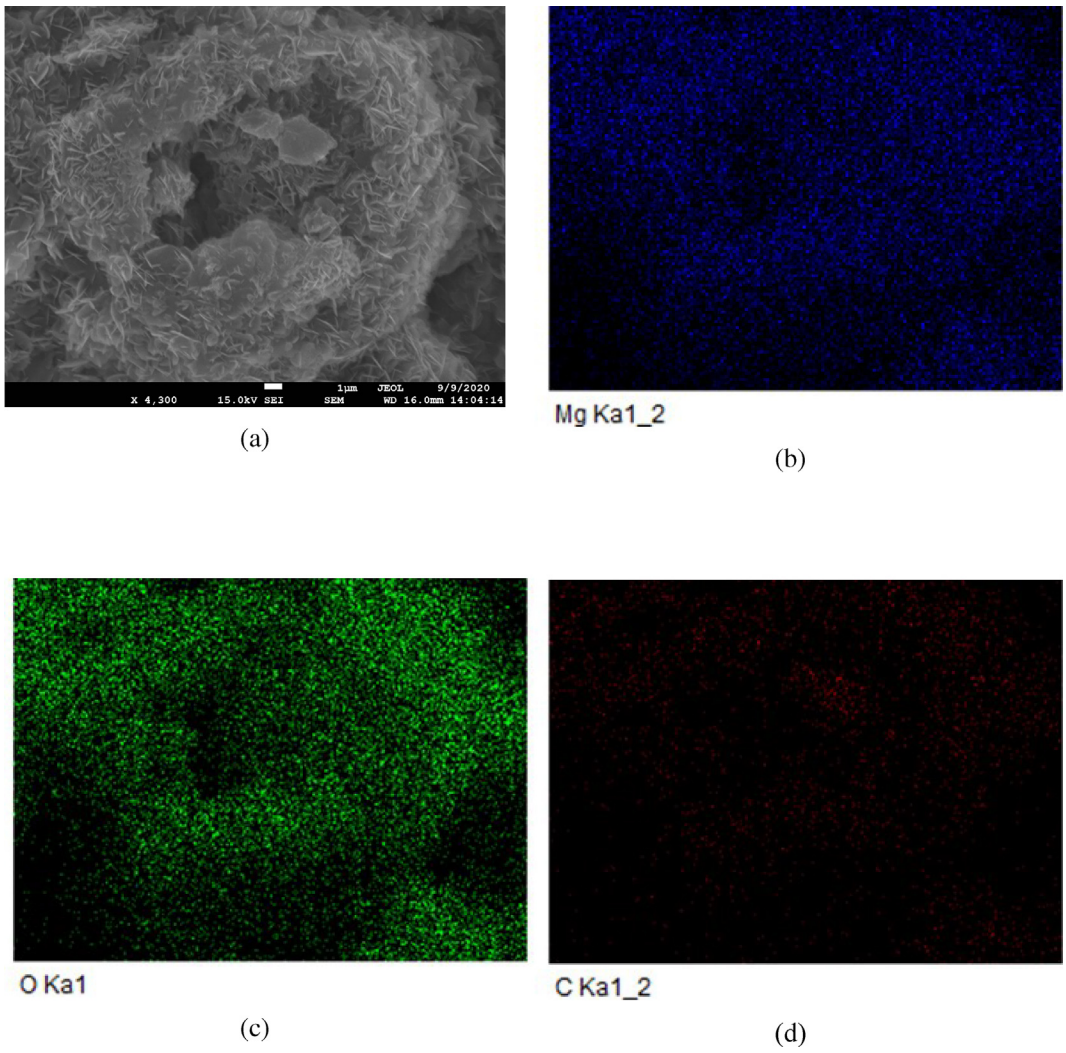

Fig. 16. Microstructural analysis of the bird nest-like structure: (a) SEM image; and EDX results showing (b) distribution of Mg, (c) distribution of O, and (d) distribution of C.

4. Conclusions

The hydration of RMC is limited by the initial formation of Mg $(OH)_2$ on the surface layer of MgO particles. This limitation results in a low hydration degree and limited strength gain within RMC formulations. The main goal of this study was to enhance the reaction and associated mechanical and microstructural properties of RMC blends by incorporating MA (i.e. hydration agent) and H and M (i.e. RMC replacements). The individual influences of each of these additives, along with the simultaneous incorporation of MA with H or M on the reaction mechanisms, phase formations and performance of RMC blends were investigated via the assessment of hydration kinetics and microstructural and mechanical analyses.

The obtained findings revealed the lower pH values of mixes containing H or M, indicating the acceleration of MgO dissolution and precipitation of hydrate phases. The larger surface area of H enabled a more pronounced acceleration of reaction kinetics, which resulted in the enhancement of the hydration of RMC, as also shown by the heat released during isothermal calorimetry. The inclusion of MA also led to reductions in the pH of sample solution. When coupled with the ability of acetate groups to enable the increased precipitation of brucite away from the MgO grains in the pore solution, RMC formulations involving MA demonstrated significantly improved hydration and associated mechanical performance.

While their individual uses also revealed enhancements in reaction mechanisms and strength development, the simultaneous inclusion of MA and M in RMC formulations enabled the acceleration of the hydration reaction, along with improvements in the morphologies of the reaction products. Accordingly, while the inclusion of M stimulated the formation of rosette-like crystals, the use of MA led to the wide-spread formation of needle-like artinite, a commonly observed Mg-carbonate phase within RMC blends. The densification of the microstructure in the presence of lower w/b ratios and the compact agglomeration of various hydrate and carbonate phases translated into a 240% increase in the strength of these samples after 7 days of curing under ambient conditions. Overall, the obtained findings revealed the benefits of partially replacing RMC with M, which enhanced the reactions and associated performance, and resulted in more sustainable mixes considering the abundant resources and lack of any CO_2 emissions associated with the production of M when compared with RMC.

Another key finding was the formation of a novel bird nest-like structure, and the presence of brucite with a low crystallinity,

along with other Mg-carbonate phases within mixes involving the use of H cured under ambient conditions. These formations were not expected as (i) previous findings usually report the formation of brucite upon the hydration of RMC and (ii) these samples were not subjected to any notable carbonation conditions to facilitate the formation of Mg-carbonates within the short curing durations used in this study. Accordingly, a potential bond between H and brucite could have changed the crystallinity of brucite and form a bird nest-like arrangement surrounding the H seeds. This unique arrangement, which has not been reported in the prior literature within the context of RMC formulations, could highlight the role of different additives in altering the formation of reaction products that enhanced the carbonation reaction and the associated formation of Mg-carbonates. Furthermore, the use of MA accelerated the hydration of RMC and the formation of needle-like crystals, as well as stimulating the formation of brucite with a higher crystallinity in RMC-H samples.

CRediT authorship contribution statement

N.T. Dung: Conceptualization, Data curation, Formal analysis, Investigation, Methodology, Writing - original draft, Writing - review & editing. **C. Unluer:** Conceptualization, Funding acquisition, Project administration, Resources, Supervision, Validation, Writing - original draft, Writing - review & editing.

Declaration of Competing Interest

The authors declare that they have no known competing financial interests or personal relationships that could have appeared to influence the work reported in this paper.

Acknowledgment

The authors would like to acknowledge the financial support from the Singapore MOE Academic Research Fund Tier 1 (RG 95/16) for the completion of this research project.

References

[1] J. Green, Calcination of precipitated Mg(OH)2 to active MgO in the production of refractory and chemical grade MgO, J. Mater. Sci. 18 (1983) 637–651.
[2] V.S.S. Birchal, S.D.F. Rocha, V.S.T. Ciminelli, The effect of magnesite calcination conditions on magnesia hydration, Miner. Eng. 13 (2000) 1629–1633.
[3] M. Liska, L.J. Vandeperre, A. Al-Tabbaa, Influence of carbonation on the properties of reactive magnesia cement-based pressed masonry units, Adv. Cem. Res. 20 (2008) 53–64.
[4] C. Sonat, C.H. Lim, M. Liska, C. Unluer, Recycling and reuse of reactive MgO cements–A feasibility study, Constr. Build. Mater. 157 (2017) 172–181.
[5] S. Ruan, C. Unluer, Comparative life cycle assessment of reactive MgO and Portland cement production, J. Cleaner Prod. 137 (2016) 258–273.
[6] L.J. Vandeperre, A. Al-Tabbaa, Accelerated carbonation of reactive MgO cements, Adv. Cem. Res. 19 (2007) 67–79.
[7] R. Hay, K. Celik, Accelerated carbonation of reactive magnesium oxide cement (RMC)-based composite with supercritical carbon dioxide (scCO2), J. Cleaner Prod. 248 (2020) 119282.
[8] E. Gartner, T. Sui, Alternative cement clinkers, Cem. Concr. Res. 114 (2018) 27–39.
[9] M. Liska, A. Al-Tabbaa, Performance of magnesia cements in porous blocks in acid and magnesium environments, Adv. Cem. Res. 24 (2012) 221–232.
[10] L. Mo, D.K. Panesar, Effects of accelerated carbonation on the microstructure of Portland cement pastes containing reactive MgO, Cem. Concr. Res. 42 (2012) 769–777.
[11] D.A. Torres-Rodríguez, H. Pfeiffer, Thermokinetic analysis of the MgO surface carbonation process in the presence of water vapor, Thermochim Acta 516 (2011) 74–78.
[12] D.K. Panesar, L. Mo, Properties of binary and ternary reactive MgO mortar blends subjected to CO2 curing, Cem. Concr. Compos. 38 (2013) 40–49.
[13] R. Hay, K. Celik, Hydration, carbonation, strength development and corrosion resistance of reactive MgO cement-based composites, Cem. Concr. Res. 128 (2020) 105941.
[14] S. Isohata, K. Watabe, M. Shimoshimizu, T. Iwaisako, Magnesia cement composition, process of its manufacture, and composite comprising same, 1975.
[15] C. Kuenzel, F. Zhang, V. Ferrándiz-Mas, C.R. Cheeseman, E.M. Gartner, The mechanism of hydration of MgO-hydromagnesite blends, Cem. Concr. Res. 103 (2018) 123–129.
[16] N.T. Dung, C. Unluer, Carbonated MgO concrete with improved performance: the influence of temperature and hydration agent on hydration, carbonation and strength gain, Cem. Concr. Compos. 82 (2017) 152–164.
[17] N.T. Dung, C. Unluer, Sequestration of CO2 in reactive MgO cement-based mixes with enhanced hydration mechanisms, Constr. Build. Mater. 143 (2017) 71–82.
[18] D.A. Vermilyea, The dissolution of MgO and Mg $(OH)_2$ in aqueous solutions, J. Electrochem. Soc. 116 (1969) 1179–1183.
[19] D. Filippou, N. Katiforis, N. Papassiopi, K. Adam, On the kinetics of magnesia hydration in magnesium acetate solutions, J. Chem. Technol. Biotechnol. 74 (1999) 322–328.
[20] K.P. Matabola, E.M. van der Merwe, C.A. Strydom, F.J.W. Labuschagne, The influence of hydrating agents on the hydration of industrial magnesium oxide, J. Chem. Technol. Biotechnol. 85 (2010) 1569–1574.
[21] L.F. Amaral, I.R. Oliveira, R. Salomão, E. Frollini, V.C. Pandolfelli, Temperature and common-ion effect on magnesium oxide (MgO) hydration, Ceram. Int. 36 (2010) 1047–1054.
[22] E.M. van der Merwe, C. Strydom, A. Botha, Hydration of medium reactive industrial magnesium oxide with magnesium acetate, J. Therm. Anal. Calorim. 77 (2004) 49–56.
[23] N.T. Dung, C. Unluer, Development of MgO concrete with enhanced hydration and carbonation mechanisms, Cem. Concr. Res. 103 (2018) 160–169.
[24] N.T. Dung, C. Unluer, Influence of accelerated hydration and carbonation on the performance of reactive magnesium oxide concrete, Adv. Cem. Res. (2018) 1–13.
[25] N.T. Dung, C. Unluer, Performance of reactive MgO concrete under increased CO2 dissolution, Cem. Concr. Res. 118 (2019) 92–101.
[26] N. Vlasopoulos, C.R. Cheeseman, Binder composition, Google Patents (2013).
[27] F. Winnefeld, E. Epifania, F. Montagnaro, E.M. Gartner, Further studies of the hydration of MgO-hydromagnesite blends, Cem. Concr. Res. 126 (2019) 105912.
[28] M.J. McKelvy, A.V.G. Chizmeshya, K. Squires, R.W. Carpenter, H. Bearat, A novel approach to mineral carbonation: enhancing carbonation while avoiding mineral pretreatment process cost, Arizona State Univ., Tempe, AZ (United States), 2006, pp. Medium: ED.
[29] S.J. Gerdemann, D.C. Dahlin, W.K. O'Connor, Carbon dioxide sequestration by aqueous mineral carbonation of magnesium silicate minerals, in: J. Gale, Y. Kaya (Eds.), Greenhouse Gas Control Technologies - 6th International Conference, Pergamon, Oxford, 2003, pp. 677–682.
[30] A. Sanna, M. Uibu, G. Caramanna, R. Kuusik, M.M. Maroto-Valer, A review of mineral carbonation technologies to sequester CO2, Chem. Soc. Rev. 43 (2014) 8049–8080.
[31] D.E. Giammar, R.G. Bruant, C.A. Peters, Forsterite dissolution and magnesite precipitation at conditions relevant for deep saline aquifer storage and sequestration of carbon dioxide, Chem. Geol. 217 (2005) 257–276.
[32] B. Garcia, V. Beaumont, E. Perfetti, V. Rouchon, D. Blanchet, P. Oger, G. Dromart, A.-Y. Huc, F. Haeseler, Experiments and geochemical modelling of CO2 sequestration by olivine: Potential, quantification, Appl. Geochem. 25 (9) (2010) 1383–1396.
[33] F. Montserrat, P. Renforth, J. Hartmann, M. Leermakers, P. Knops, F.J.R. Meysman, Olivine dissolution in seawater: implications for CO2 sequestration through enhanced weathering in coastal environments, Environ. Sci. Technol. 51 (2017) 3960–3972.
[34] S. Pacala, R. Socolow, Stabilization wedges: solving the climate problem for the next 50 years with current technologies, Science 305 (2004) 968–972.
[35] Y. Jia, B. Wang, Z. Wu, J. Han, T. Zhang, L.J. Vandeperre, C.R. Cheeseman, Role of sodium hexametaphosphate in MgO/SiO2 cement pastes, Cem. Concr. Res. 89 (2016) 63–71.
[36] K. Wang, A. Mishulovich, S.P. Shah, Activations and properties of cementitious materials made with cement-kiln dust and class F fly ash, J. Mater. Civ. Eng. 19 (2007) 112–119.
[37] S. Manso, A. Aguado, A review of sample preparation and its influence on pH determination in concrete samples, Materiales de Construcción 67 (325) (2017) 108.
[38] V. Räsänen, V. Penttala, The pH measurement of concrete and smoothing mortar using a concrete powder suspension, Cem. Concr. Res. 34 (2004) 813–820.
[39] ASTM C1702 – 15a, Standard test method for measurement of heat of hydration of hydraulic cementitious materials using isothermal conduction calorimetry, ASTM Committee C01, West Conshohocken, PA 19428-2959, United States, 2015, pp. 8.
[40] ASTM C109/C109M – 13, Standard test method for compressive strength of hydraulic cement mortars (using 2-in. or [50-mm] cube specimens), ASTM Committee C01, West Conshohocken, PA 19428-2959, United States, 2013, pp. 10.
[41] N.C. Collier, J.H. Sharp, N.B. Milestone, J. Hill, I.H. Godfrey, The influence of water removal techniques on the composition and microstructure of hardened cement pastes, Cem. Concr. Res. 38 (2008) 737–744.

[42] T. Hoang, N.T. Dung, C. Unluer, J. Chu, Use of microbial carbonation process to enable self-carbonation of reactive MgO cement mixes, Cem. Concr. Res. 143 (2021) 106391.
[43] N.T. Dung, T.J.N. Hooper, C. Unluer, Improving the carbonation resistance of Na2CO3-activated slag mixes via the use of reactive MgO and nucleation seeding, Cem. Concr. Compos. 115 (2021) 103832.
[44] H.P. Klug, L.E. Alexander, X-ray diffraction procedures, (1954).
[45] N.T. Dung, R. Hay, A. Lesimple, K. Celik, C. Unluer, Influence of CO2 concentration on the performance of MgO cement mixes, Cem. Concr. Compos. 115 (2021) 103826.
[46] Y. Sawada, K. Uematsu, N. Mizutani, M. Kato, Thermal decomposition of hydromagnesite 4MgCO3·Mg(OH)2·4H2O, J. Inorg. Nucl. Chem. 40 (1978) 979–982.
[47] L.A. Hollingbery, T.R. Hull, The thermal decomposition of natural mixtures of huntite and hydromagnesite, Thermochim Acta 528 (2012) 45–52.